Chapter 6

Background estimation

A reliable estimation of the expected SM background rates in the SRs is crucial for exercising the statistical machinery laid out in chapter 3 and making conclusive statistical statements. The background estimation approaches used in the following either rely on semi-data-driven techniques or on MC-only estimations. As estimating backgrounds only from MC simulation is often problematic due to e.g. mis-modelings in the phase space regions targeted not appropriately covered by the uncertainties, a (semi-)data-driven approach is often favoured. In the following, the major backgrounds $t\bar{t}$, single top and W + jets are estimated using a semi-data-driven approach, while the expected rates from the remaining smaller backgrounds rely purely on MC simulations and are normalised to their theoretical cross section.

6.1 General strategy

6.1.1 Transfer factor approach

Estimating background contributions in SRs in a semi-data-driven approach usually involves the introduction of so-called control regions (CRs) used to control dominant background processes by comparing their expected event rates to data. The CRs are designed to be enriched in events of a given background process (or type) while being approximately free of signal contamination. If $N_p^{\mathrm{MC}}(\mathrm{SR})$ and $N_p^{\mathrm{MC}}(\mathrm{CR})$ are the expected rates for a given background process p obtained from MC simulation in a given SR and CR, respectively, then the transfer factor $N_p^{\mathrm{MC}}(\mathrm{SR})/N_p^{\mathrm{MC}}(\mathrm{CR})$ allows to convert the number of observed background events in the CRs, $N_p^{\mathrm{obs.}}(\mathrm{CR})$, into a background estimate in the SRs, $N_p^{\mathrm{est.}}(\mathrm{SR})$, through

$$N_p^{\mathrm{est.}}(\mathrm{SR}) = N_p^{\mathrm{obs.}}(\mathrm{CR})\frac{N_p^{\mathrm{MC}}(\mathrm{SR})}{N_p^{\mathrm{MC}}(\mathrm{CR})} = \mu_p N_p^{\mathrm{MC}}(\mathrm{SR}). \tag{6.1}$$

Here, μ_p is the process-specific normalisation factor introduced in section 3.1. An important benefit of this approach is that the impact of systematic uncertainties on the estimated background rates can be evaluated on the transfer factors, that are ratios of MC estimates. As such, systematic uncertainties can cancel in the extrapolation to the SR. The uncertainty on the background estimate is then a combination of statistical uncertainties in the CR and remaining

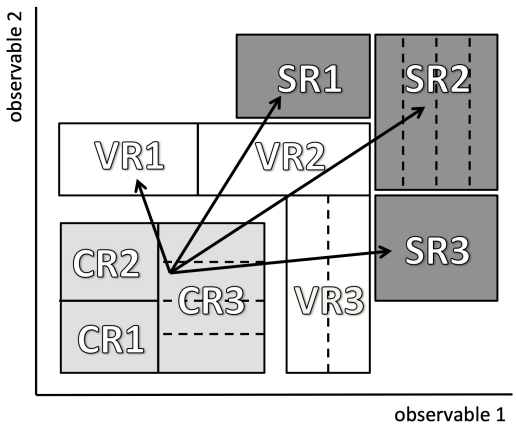

Figure 6.1: Schematic view of an analysis strategy including multiple control, validation and signal regions with one or multiple bins each. Extrapolations from the control regions into the signal regions can be verified in the validation regions lying in the phase space extrapolated over. All regions are designed to be statistically independent. Figure adapted from [154].

uncertainties affecting the extrapolation. For this reason, CRs are usually deliberately chosen to have large statistics, effectively reducing the uncertainties on the extrapolation to the SRs.

As indicated in eq. (6.1), the transfer factor approach is formally equivalent to using the process-specific normalisation factors from section 3.1, effectively *normalising* the number of total background events expected from MC to the number of observed events in each control region. In the profile likelihood fits used in the following, implemented using HistFitter [154], the normalisation factors μ_p are fitted to data instead of the background processes as expected from MC simulation. Multiple disjoint CRs are used to simultaneously normalise multiple background processes to data in a combined fit. In order not to have an underdetermined minimisation problem, at least the same number of CRs as normalisation factors need to be used. Two different profile likelihood fit configurations are used in the following. The first configuration is a so-called *background-only* fit configuration assuming no signal contribution and typically only including the CRs. The second configuration is a so-called *model-dependent* fit configuration with nominal signal contribution using CRs as well as SR.

In order to verify the quality of the extrapolation from the CRs to the SRs, so-called validation regions (VRs) are defined. VRs do not participate in the actual fit of the model parameters to data, but serve as intermediate regions to verify the extrapolation. For this reason, VRs are typically placed in the region between the CRs and SRs that is extrapolated over. A schematic view of an analysis strategy using all three types of regions is shown in fig. 6.1. All three types of regions can have more than one bin and are separated using suitable observables that are extrapolated over. In order to be able to use information from all control and signal regions in a single profile likelihood fit, all regions necessarily need to be statistically independent.

6.1.2 Analysis blinding

An important concept in the design phase of searches for new physics is the idea of *blinding* regions of interest [238], meaning that measured data are not looked at in these regions. This avoids issues of *experimenter's bias*, i.e. unintended influences on the design of the analysis based on the observed data. If data were already known when designing the signal regions (and therefore the outcome of the analysis would be known to some extent), experimenter's bias could for example occur during the selection of the final signal region definitions.

During the design of a search for SUSY, signal regions are generally kept blinded until the complete analysis strategy is fixed. Once the SRs have been designed, the next step is to develop a suitable background estimation strategy, often involving the introduction of CRs with negligible signal contamination. This is then often followed by the design of VRs that can be unblinded once the CRs are fixed. The SRs are only unblinded after the extrapolation of the background estimate from the CRs has been verified in the VRs, allowing to either quantify potential excesses in data or set limits on model parameters.

6.1.3 Data versus Monte Carlo plots

In this chapter, all plots comparing data versus MC are so-called *pre-fit* plots, meaning that no background-only fit has been run in order to determine the normalisation factors and total systematic uncertainties for the background estimate. The contributions from the dominant backgrounds $t\bar{t}$, W + jets and single top are normalised simultaneously in the control regions by solving the system of i equations

$$n_{\text{data}}^{\text{CR}_i} = \mu_{t\bar{t}} B_{t\bar{t}}^{\text{CR}_i} + \mu_W B_W^{\text{CR}_i} + \mu_{\text{ST}} B_{\text{ST}}^{\text{CR}_i} + B_{\text{other}}^{\text{CR}_i}, \tag{6.2}$$

where i runs over the list of CRs introduced in section 6.2 and $\mu_{t\bar{t}}$, μ_{W} and μ_{ST} are the normalisation factors of the $t\bar{t}$, W + jets and single top backgrounds, respectively, that are to be determined. $B_{t\bar{t}}^{\text{CR}_i}$, $B_{\text{ST}}^{\text{CR}_i}$, $B_{\text{ST}}^{\text{CR}_i}$ and $B_{\text{other}}^{\text{CR}_i}$ are the background rates expected from MC simulation in the i-th CR. The normalisation factors obtained are 0.96 for $t\bar{t}$, 1.24 for W + jets and 0.73 for single top. As will be shown in section 8.1, the normalisation factors obtained using the full statistical procedure will be close to these values.

Additionally, the uncertainty bands on the background estimate will include only MC statistical uncertainty as well as experimental uncertainties. The variations of the experimental uncertainties are normalised to the nominal background estimate in the case of $t\bar{t}$, W + jets and single top, such that only the shapes of the dominant backgrounds are affected. For the remaining minor backgrounds, the experimental uncertainties can affect both normalisation and shape. All experimental uncertainties are assumed to be fully correlated over all processes and bins, allowing them to summed in quadrature. Finally, the uncertainty bars on the data points are obtained by assuming data to be Poisson distributed and correspond to the 68% confidence interval.

6.2 Control regions

The contributions from $t\bar{t}$, W + jets production and single top processes are normalised to data in dedicated control regions. Other processes like Z + jets, diboson and multiboson, $t\bar{t}+V$, $t\bar{t}+h$ and $V+h$ are estimated directly from MC simulation and normalised to their theoretical cross sections. All CRs are designed to be kinematically as close as possible to the respective SRs, such that the normalisation factors derived in the CRs are also valid in the SRs. The CRs are mutually exclusive and made orthogonal to the SRs through their requirements on m_{T}, m_{CT} and $m_{b\bar{b}}$. Apart from the requirements on these three observables as well as the requirement on $m_{\ell b_1}$ (removed altogether in the CRs), the CRs share the same set of cuts as the SRs. Figure 6.4(a) illustrates the configuration of all CRs, especially highlighting the fact

Table 6.1: Overview of the CR and VR definitions. All regions partially share the same selection as the SR for all variables except $m_{\ell b_1}$, which is not used in the CR and VR definitions.

CR	**TR-LM**	**TR-MM**	**TR-HM**	**WR**	**STR**	
$m_{b\bar{b}}$ [GeV]		<100 or >140		$\in [50, 80]$	>195	
m_{T} [GeV]	$\in [100, 160]$	$\in [160, 240]$	>240	$\in [50, 100]$	>100	
m_{CT} [GeV]		<180		>180	>180	
VR	**VR-onLM**	**VR-onMM**	**VR-onHM**	**VR-offLM**	**VR-offMM**	**VR-offHM**
$m_{b\bar{b}}$ [GeV]		$\in [100, 140]$		$\in [50, 80] \cup [160, 195]$	$\in [50, 80] \cup [160, 195]$	$\in [50, 75] \cup [165, 195]$
m_{T} [GeV]	$\in [100, 160]$	$\in [160, 240]$	>240	$\in [100, 160]$	$\in [160, 240]$	>240
m_{CT} [GeV]		<180			>180	

that all CRs are located in sideband regions off the $m_{b\bar{b}}$ window, significantly reducing signal contamination. Table 6.1 summarises the kinematic requirements separating the CRs from other regions of interest in the analysis.

Control regions for $t\bar{t}$

As events from $t\bar{t}$ processes constitute the dominant SM background in all SRs, it is necessary to have a precise and reliable estimation of their contributions. Three CRs are defined for $t\bar{t}$, following the same binning in m_{T}, and thus called TR-LM, TR-MM and TR-HM in the following. A good purity of $t\bar{t}$ processes as well as the necessary high MC statistics are achieved by inverting the requirement on m_{CT}, selecting events below the kinematic endpoint for $t\bar{t}$ processes. The achieved pre-fit $t\bar{t}$ purities are 79.6% in TR-LM, 85.9% in TR-MM and 84.1% in TR-HM. The remaining contributions stem mostly from single top and W + jets processes and vary between 8.6%–14.1% and 1.8%–4.3%, respectively, depending on the bin in m_{T}.

For a trustworthy estimate of the contribution from $t\bar{t}$ processes, it is important that the control regions associated to each signal region exhibit approximately the same composition of $t\bar{t}$ decay modes. The decay mode most relevant at relatively low and moderate values of m_{T} is the semi-leptonic decay ($\ell\nu qq$) where one of the W bosons decays leptonically, while the other one undergoes a hadronic decay. The semi-leptonic decay mode exhibits the well-known kinematic endpoint in m_{T} and thus quickly loses importance at high transverse mass values. Events involving a hadronic decay of a τ-lepton originating from $W \to \tau_{\mathrm{had}}\nu$ in one of the two branches and a leptonic W boson decay in the other branch ($\ell\nu\tau_{\mathrm{had}}\nu$), are the dominant decay mode in selections with high values of m_{T}. Due to the additional neutrino in such events, the $\ell\nu\tau_{\mathrm{had}}\nu$ decay mode does not exhibit the same kinematic endpoint as the semi-leptonic one. Finally, di-leptonic decays ($\ell\nu\ell\nu$) and events with a leptonically decaying τ-lepton ($\ell\nu\tau_{\ell}\nu$) where one of the two leptons is not reconstructed play a sub-dominant role in all regions. Other $t\bar{t}$ decay modes play a negligible role in all analysis selections.

In the low-mass regions with moderate values in m_{T} close to its kinematic endpoint, 80% (40%) of $t\bar{t}$ events involve the semi-leptonic decay mode in the control region (signal region). The sub-dominant decay mode in TR-LM and SR-LM involves the $\ell\nu\tau_{\mathrm{had}}\nu$ decay mode, with a contribution of 25% and 10%, respectively. Di-leptonic and $\ell\nu\tau_{\ell}\nu$ decay modes each contribute about 15% of all events in TR-LM and about 3% in SR-LM. Thus, the composition in the low-mass regions is not exactly the same in the control and signal regions, but the agreement is

considered to be acceptable for a trustworthy background estimate. With about 45% (36%) and 30% (35%), the largest contributions in TR-MM (SR-MM) originate from $\ell\nu\tau_{\text{had}}\nu$ decays and di-leptonic events, respectively. Events with a $\ell\nu\tau_{\ell}\nu$ decay contribute to about 10% (15%) in TR-MM (SR-MM). In the high-mass control and signal regions with a high requirement on m_{T}, the majority (about 50%) of events involve the $\ell\nu\tau_{\text{had}}\nu$ decay mode, while the di-leptonic and $\ell\nu\tau_{\text{had}}\nu$ decay modes contribute with about 30% and 20%, respectively. Overall, the compositions of the different $t\bar{t}$ decay modes in each control region are thus similar to the contributions in the respective signal region, meaning that the $t\bar{t}$ processes constrained through the log-likelihood fit in the CRs are the same as those to be estimated in the SRs.

Signal contamination is additionally avoided by inverting the requirement on $m_{b\bar{b}}$, i.e. placing the $t\bar{t}$ CRs in the $m_{b\bar{b}}$ sideband. The maximum signal contamination over the entire signal grid is 0.8%, 1.1% and 1.9% for TR-LM, TR-MM and TR-HM, respectively, and thus negligible. Figures 6.3(a) to 6.3(c) show the signal contamination over the entire signal grid.

Control region for W + jets

Events from W + jets production represent the second largest contribution of SM background processes in most SRs. A single W + jets control region, called WR in the following, is defined by replacing the signal region requirements on m_{T} and $m_{b\bar{b}}$ with $50\,\text{GeV} < m_{\text{T}} < 100\,\text{GeV}$ and $50\,\text{GeV} < m_{b\bar{b}} < 80\,\text{GeV}$, respectively. No bins in m_{CT} are defined for WR.

Applying a low requirement on m_{T} allows to predominantly select events in front of the kinematic endpoint of the transverse mass of the W boson, resulting in a high statistics control region with a pre-fit W +jets purity of roughly 52.5%. The sub-dominant background component of WR is $t\bar{t}$ with 35.2%. Minor contributions of 7.0% and 4.2% originate from single top and diboson processes, respectively. The composition of W +jets events in WR and all signal regions is found to be dominated by W boson production in association with HF decays with 2 real b-jets. Minor contributions originate from HF decays with mis-tagged c-quarks or processes with mis-tagged light-flavour jets.

As was the case for the $t\bar{t}$ control regions, placing WR off the Higgs mass peak allows to achieve a tolerable maximum signal contamination of about 2.4% without affecting the composition of processes in the W + jets background too much. Most signal points have significantly less than 1% signal contamination in WR. The signal contamination throughout the entire signal grid is shown in fig. 6.3(d).

Control region for single top

Single top processes result in significant background contributions in some SRs, necessitating a proper semi-data-driven estimation. A single top CR (STR) is defined by replacing the Higgs mass window cut on $m_{b\bar{b}}$ with $m_{b\bar{b}} > 195\,\text{GeV}$ and removing the bins in m_{CT}.

Placing STR in the off the Higgs boson mass peak achieves a low maximum signal contamination of roughly 0.8%. The signal contamination across the entire signal grid is shown in fig. 6.3(e). The pre-fit purity of the single top processes in STR is 51.7%. Sub-dominant contributions arise from $t\bar{t}$ processes (29%), W + jets (10%) and $t\bar{t} + V$ (6%) production.

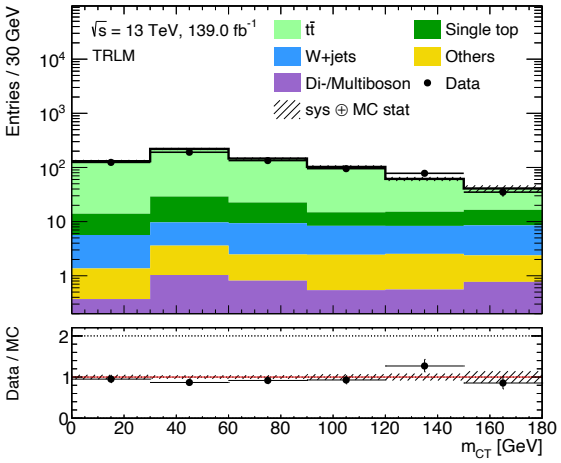

(a) TRLM

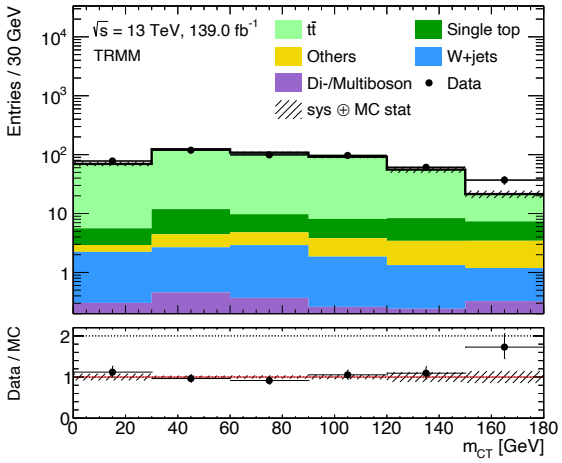

(b) TRMM

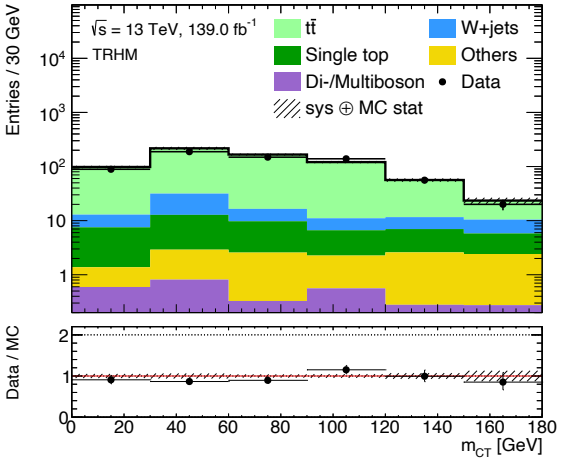

(c) TRHM

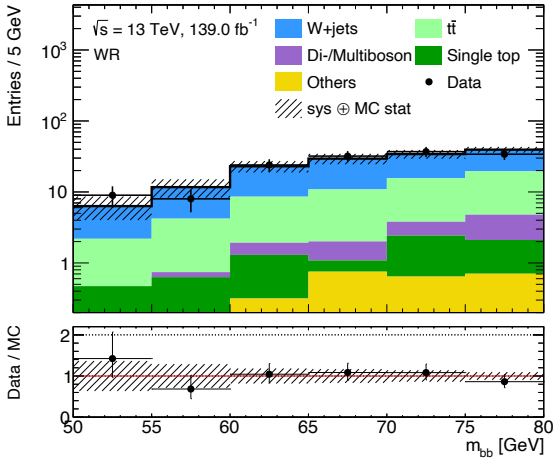

(d) WR

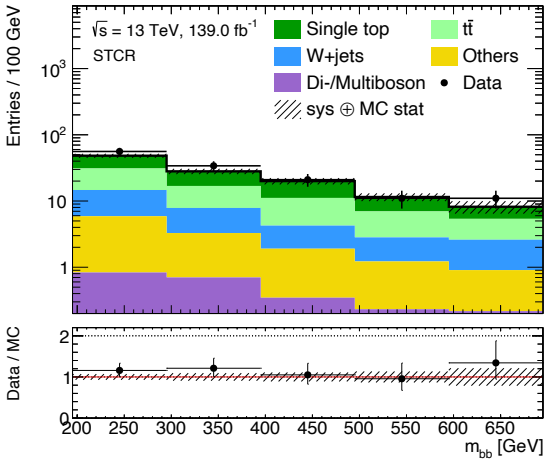

(e) STCR

Figure 6.2: Exemplary distribution shown in each control region. As laid out in the beginning of this chapter, the shaded region includes MC statistical uncertainty as well as experimental uncertainties, added in quadrature. A good agreement between MC expectation and data is observed in all CRs.

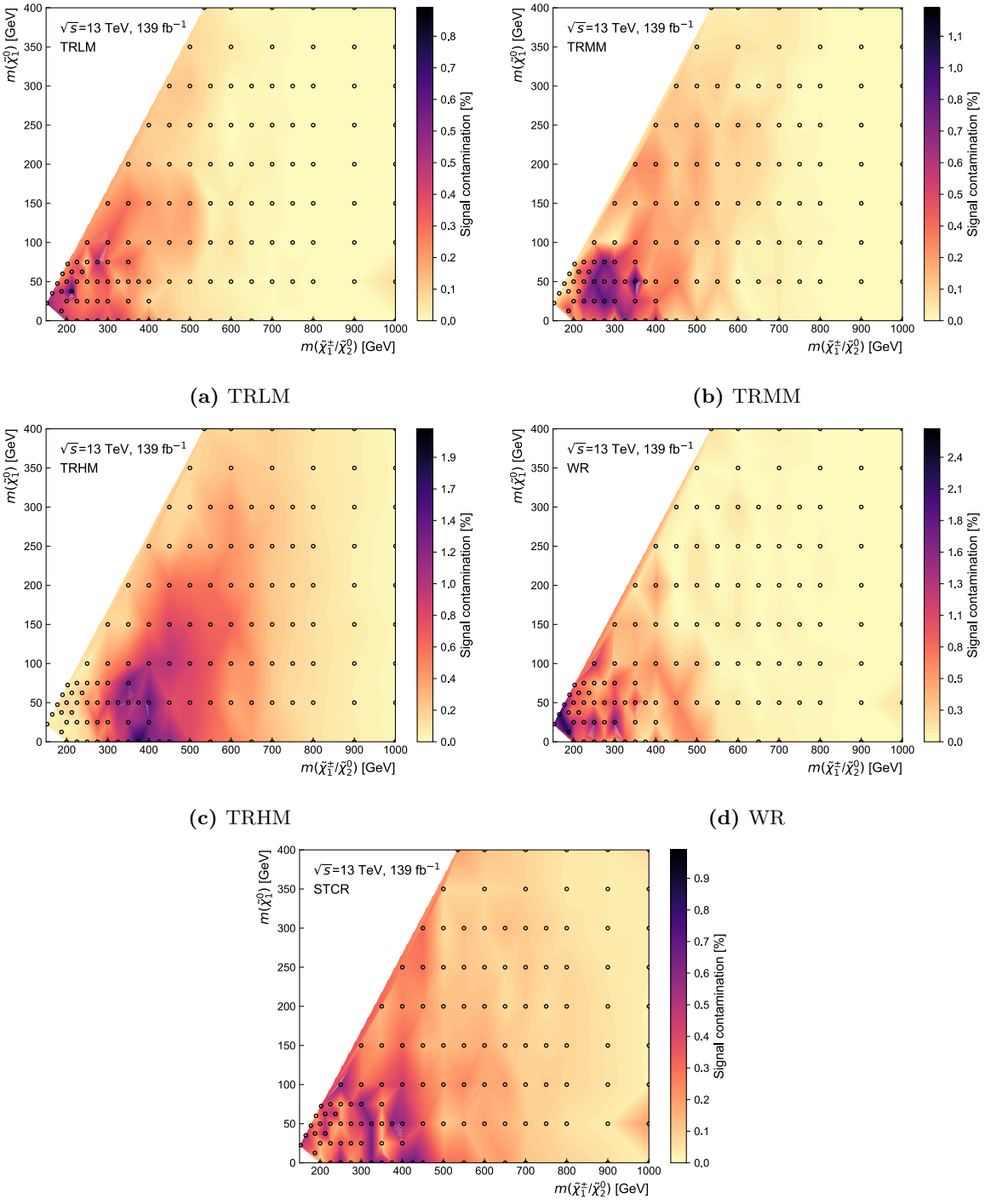

(a) TRLM **(b)** TRMM

(c) TRHM **(d)** WR

(e) STCR

Figure 6.3: Signal contamination (shown on the *z-axis*) for all CRs throughout the signal grid. The space between the signal points (indicated by the black circles) is interpolated using Delaunay triangles.

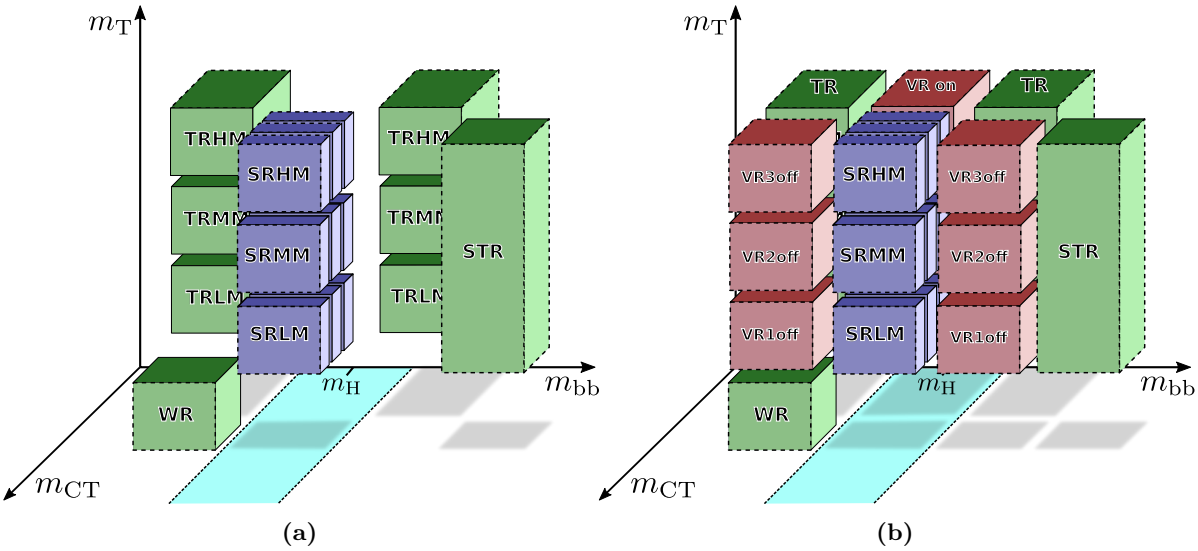

Figure 6.4: Configuration of (a) the control regions placed around the signal regions off the $m_{b\bar{b}}$ window as well as (b) the validation regions in the phase space between the CRs and SRs. The VRs are arranged such that each of the extrapolations can be validated.

6.3 Validation regions

Two sets of VRs regions are introduced in order to verify the extrapolation over the different distributions. The selections defining all VRs are summarised in table 6.1. The first set, called VR-on is situated on the Higgs boson mass peak but with the m_{CT} requirement inverted to $m_{\mathrm{CT}} < 180\,\mathrm{GeV}$. This allows the VR-on regions to validate the extrapolation over m_{CT}, performed when extrapolating the background estimate from the $t\bar{t}$ control regions into the signal regions. Three VR-on regions are defined by requiring the same binning in m_{T} as already used for the signal regions. This allows each of the VR-on regions, called VR-onLM, VR-onMM and VR-onHM, to act as validation region for the respective signal region. A similar composition of $t\bar{t}$ decay modes as in the control and signal regions is observed in the VR-on regions, necessary for a trustworthy validation of the $t\bar{t}$ estimate. A maximum signal contamination of about 5%–14% is achieved, depending on the requirement in m_{T}. As can be seen from fig. A.9, most signal points have a signal contamination well below 5% for all VR-on regions.

The second set of VRs is located on both sides off the Higgs boson mass peak at same values in m_{CT} than the SRs. This set of *off-peak* VRs, called VR-off, is used to validate the extrapolation in $m_{b\bar{b}}$ and m_{T}. Similar to the on-peak validation regions, the VR-off regions are split into bins in m_{T} matching the signal regions. The resulting validation regions VR-offLM, VR-offMM and VR-offHM, can thus be used to validate the background estimate in their respective signal region. The maximum signal contamination in the VR-off regions is found to be about 7%–13%, depending on the requirement on m_{T}. Most signal points, however, reveal a signal contamination in the VR-off regions of less than 3% (cf. fig. A.9).

Chapter 7

Systematic uncertainties

Several sources of systematic uncertainties need to be considered in the following. As laid out in chapter 3, they enter the likelihood as nuisance parameters and can be interpreted as a loss of information on the signal strength parameter. In the following, they are separated into experimental uncertainties arising from finite detector resolution and object reconstruction and theoretical uncertainties due to modelling of the physics processes during simulation.

7.1 Experimental uncertainties

Experimental uncertainties arise from the experimental methods used to derive the signal and background rate estimations. They are evaluated using up and down variations provided either as variational weights in the case of efficiency uncertainties, or as additional variational samples derived by performing the object reconstruction with varied parameters.

7.1.1 Pile-up reweighting and luminosity

The MC events were largely already generated before the full data was taken, and therefore before the full pileup profile in data was known. For this reason, the number of average interactions $\langle\mu\rangle$ per bunch crossing in MC is in general not identical to that in data, necessitating a reweighting procedure in MC. In order to account for differences in the measured inelastic pp cross sections and the one obtained from MC simulation, a scale factor of 1.03 is applied before the reweighting procedure. As MC samples are generated with integer of $\langle\mu\rangle$ only, the scale factor is applied to data instead. The uncertainty on the pileup reweighting is evaluated by varying the data scale factor by ± 0.04 and deriving variational pileup weights.

As detailed in section 2.1.2, the total integrated luminosity relies on the measurement of the bunch luminosity which in turn needs precise measurements of the visible inelastic cross section σ_{vis} as well as the visible pile-up parameter μ_{vis}. Uncertainties on the measurement of the total recorded cross section are dominated by the uncertainties on σ_{vis} that is measured during special vdM scans. For the full Run 2 dataset, an overall luminosity uncertainty of $\pm 1.7\%$, is considered for all MC processes not normalised to data using a CR, derived using the methods described in Ref. [100].

7.1.2 Triggers

As all selections considered in the analysis apply a minimum $E_{\mathrm{T}}^{\mathrm{miss}}$ requirement of 240 GeV where the $E_{\mathrm{T}}^{\mathrm{miss}}$ triggers are fully efficient (see section 4.7), a 2% normalisation uncertainty correlated over all bins is considered.

7.1.3 Leptons

A large number of uncertainties on electrons arises from energy scale and resolution measurements [208, 210]. They are assumed to be fully correlated in η and are summed in quadrature, resulting in one nuisance parameter for the energy scale and one for the resolution. Similarly, uncertainties on muons arise from calibrations of the muon momentum scale and resolution [211]. They are evaluated using variations in the smearing of the ID and MS tracks as well as the momentum scale, resulting in a total of five nuisance parameters entering the likelihood. Additional lepton uncertainties considered in the following originate from reconstruction, identification and isolation efficiencies, as well as track-to-vertex association and bad muon identification efficiencies. The latter two are only considered for muons.

7.1.4 Jets

The calibration of the jets to the absolute JES is subject uncertainties arising e.g. from the *in situ* measurements, pile-up effects or flavour-dependence [216], encoded in a large set of 125 parameters. The full detail contained in the complete set of uncertainty components offers far greater statistical precision than needed for the following analysis. As the majority of the parameters (a total of 98) stems from *in situ* measurements, an eigenvector decomposition is performed on the covariance matrix of these components [239], allowing to determine the 15 principal orthogonal components (including a residual term adding the remaining terms in quadrature), with minimal loss in bin-by-bin correlation information. Five additional parameters evaluating uncertainties arising from *in situ* η-intercalibrations of forward jets with respect to central jets are kept separate due to their two-dimensional dependence on p_{T} and η [216]. Effects from pile-up are described by four nuisance parameters. Uncertainties arising from differing detector responses to gluon- and quark-initiated jets as well as flavour-related differences are accounted for by two more nuisance parameters. Uncertainties from jets that are not contained in the calorimeters and *punch-through* into the MS are evaluated with an additional parameter. A last parameter encodes the uncertainty arising from the calibration of MC samples reconstructed using ATLFAST-II instead of the full detector simulation.

Systematic uncertainties on the JER arise from measured differences between data and MC simulation, noise from pile-up, and *in situ* measurements of the jet p_{T} imbalance. A similar eigenvector decomposition as for part of the JES uncertainties is used, reducing the set of nuisance parameters considered in the following to 13 [216]. Finally, uncertainties related to the efficiency of jet vertex tagging are evaluated using a weight systematic.

7.1.5 Flavour tagging

Uncertainties on the flavour tagging efficiency originate e.g. from modelling uncertainties as well as uncertainties on the reconstruction of physics objects. As for the JER and JES the full set of nuisance parameters that would in principle need to be included in order to consider the full bin-by-bin correlations and p_{T} and η dependence of the uncertainties, is reduced to a more manageable size using an eigenvector decomposition. This leads to a total of five nuisance parameters encoding uncertainties on the b-tagging efficiency, c-jet and light-jet mistagging rate as well as the extrapolation to high-p_{T} jets [222, 223].

7.1.6 Missing transverse energy

The uncertainties on $E_{\mathrm{T}}^{\mathrm{miss}}$ are evaluated using the systematic variations of all calibrated objects as inputs to the $E_{\mathrm{T}}^{\mathrm{miss}}$ calculation. Additional uncertainties arise from the calculation of the track soft term. In the following, uncertainties on the soft term scale and resolution are considered, resulting in one nuisance parameter for the soft term scale and two nuisance parameters (corresponding to the perpendicular and parallel components) for the soft term resolution uncertainty. All track soft term uncertainties are derived by comparing simulation to $Z \to \mu\mu$ events [224]. Contributions to the JES uncertainty due to pile-up is considered

7.2 Theoretical uncertainties

As discussed in section 2.2.8, due to finite order calculations, the different steps of the MC simulation generally introduces a certain number of unphysical scales and parameters. In order to quantify the uncertainties arising from the ad-hoc values of these, the MC simulation generally needs to be re-run with systematically varied parameter values. Since varied MC simulation parameters affect the event kinematics even before reconstruction and calibration, it is computationally very expensive to produce a full set of variations for each MC sample used in the nominal analysis.

In the following, multiple approaches are used to derive the theory uncertainties. For some of the variational samples, the full MC simulation chain was run with reduced statistics or different samples produced with a different set of MC generators and tunes were available. For others, variations were already processed during the initial MC simulation of the nominal sample and subsequently stored as variational weights. Finally, some of the variational samples were simulated at truth-level (i.e. without detector simulation). The latter approach was used especially in the case of SUSY signal samples, where theory uncertainties are expected to only have a minor impact and a full simulation of all parameter variations would be computationally unfeasible.

For background processes that are normalised to data in a dedicated CR, the theory uncertainties are evaluated on the transfer factors. For a process p, a control region CR_i, and a destination region R_j (either a SR or a VR), the transfer factor reads

$$f_p(\mathrm{CR}_i \to \mathrm{R}_j) = \frac{N_p^{\mathrm{MC}}(\mathrm{R}_j)}{N_p^{\mathrm{MC}}(\mathrm{CR}_i)}, \tag{7.1}$$

where $N_p^{\mathrm{MC}}(\mathrm{R}_j)$ and $N_p^{\mathrm{MC}}(\mathrm{CR}_i)$ are the expected event rates for the process p in CR_i and R_j, respectively. The systematic uncertainty on the transfer factor is then given by

$$\Delta f_p^{\mathrm{syst}} = \frac{f_p^{\mathrm{variation}}}{f_p^{\mathrm{nominal}}} - 1, \tag{7.2}$$

with $f_p^{\mathrm{variation}}$ and f_p^{nominal} the transfer factors from the variational and nominal samples, respectively. If the MC samples used for deriving the variational and nominal transfer factors are statistically independent, a statistical component of the uncertainty is derived using the individual statistical uncertainties on the background estimate,

$$\Delta f_p^{\mathrm{stat}} = (\Delta f_p^{\mathrm{syst}} + 1)\sqrt{\sum_{n\in\boldsymbol{N}} (\frac{\sigma_n}{n})^2}, \tag{7.3}$$

where n runs over the set of expected event rates and σ_n is the absolute MC statistical uncertainty associated to each expected event rate n. In the following the control region used to evaluate the uncertainties on the transfer factors is taken to be the sum of all CRs introduced in section 6.2. This not only significantly improves the statistics in the region used for normalisation, but also results in a consistent treatment across all theoretical uncertainties on all relevant processes.

For other backgrounds directly estimated from MC simulation, the systematic uncertainty on the expected event rate in each region R_i is given by

$$\Delta n_p^{\mathrm{syst}}(\mathrm{R}_i) = \frac{n_p^{\mathrm{syst}}(\mathrm{R}_i) n_p^{\mathrm{nominal}}(\mathrm{P})}{n_p^{\mathrm{nominal}}(\mathrm{R}_i) n_p^{\mathrm{syst}}(\mathrm{P})} - 1, \tag{7.4}$$

where the region P is a so-called *loose preselection* with minimal analysis selection criteria used for normalisation of the event rates to be compared. If not otherwise indicated the loose preselection used for normalisation requires exactly one isolated lepton, 2–3 jets of which at least one is b-tagged, $E_{\mathrm{T}}^{\mathrm{miss}} > 220\,\mathrm{GeV}$ and $m_{\mathrm{T}} > 50\,\mathrm{GeV}$.

Apart from the hard scattering and parton showering uncertainties on top processes, all other theoretical uncertainties enter the likelihood as asymmetric correlated shape uncertainties. The hard scattering and parton showering uncertainties on top processes described below are estimated using MC generator comparisons and thus need to be symmetrised. The shape information is however still kept, i.e. the uncertainties are not one-sided.

7.2.1 Background

$t\bar{t}$ and single top

Theory uncertainties on the estimate of $t\bar{t}$ and single top processes arise for example from the simulation of the hard scattering between the interacting partons. These are evaluated by comparing the nominal MC samples generated using Powheg and Pythia8 with alternative samples generated using MadGraph_aMC@NLO and Pythia8. An uncertainty resulting from the hadronisation and fragmentation scheme chosen in Pythia8 is estimated by comparison to a MC sample generated using Powheg and Herwig++ [240]. Uncertainties arising from ISR are evaluated at full reconstruction level by varying up and down by a factor of two the

unphysical renormalisation μ_R and factorisation μ_F scales as well as the parameters controlling the showering and ME+PS matching [241]. Likewise, uncertainties arising from simulation of FSR are estimated by varying the effective coupling α_s^{FSR} [241].

Uncertainties also originate from the PDF set used when simulating the nominal MC sample. As detailed in table 4.1, the NNPDF3.0NLO is used for the simulation of both $t\bar{t}$ and single top processes. An envelope around the variational expected event rates obtained from the NNPDF3.0NLO uncertainties are used to compute an uncertainty on the transfer factor.

Beyond LO single top production diagrams, interference appears between Wt and $t\bar{t}$ production. Two approaches are commonly used to try and isolate the Wt channel: diagram removal (DR) and diagram subtraction (DS) [242]. While the former removes all diagrams in the NLO Wt amplitude that are doubly resonant (meaning that they involve an intermediate t quark that can be on-shell), the latter introduces subtraction terms in the NLO Wt cross section cancelling the $t\bar{t}$ contribution [242]. As the DR scheme is used for estimating the event rate of the Wt channel in the analysis, a comparison with an estimation using the DS scheme allows to derive an uncertainty associated to the interference.

W/Z + jets

For W/Z + jets processes, simulated using Sherpa 2.2.1, four different unphysical scales can be varied in order to investigate uncertainties on the modelling. The renormalisation μ_R and factorisation μ_F scales are both independently and together varied up and down by a factor of two, resulting in a total of seven combined variations. Three envelopes are determined from varying only μ_R, only μ_F or μ_R and μ_F together, allowing to determine three separate uncertainties. The CKKW ME+PS matching scheme also uses an unphysical scale for determining the overlap between jets from the ME and the PS. The nominal value of 20 GeV for the merging scale is varied to 30 GeV and 15 GeV for the up and down systematic variations, respectively. Finally, the scale used for resummation of soft gluon emission, μ_{QSF} is varied up and down by a factor of two.

An additional uncertainty arises from the choice of PDF set used for simulating W/Z + jets. It is evaluated by propagating the PDF error set (containing slightly different parameterisations of the PDF) to the analysis observables. Uncertainties due to the choice of $\alpha_s = 0.118$ for fitting the PDFs are estimated by comparing with variations using $\alpha_s(m_Z) = 0.119$ and $\alpha_s(m_Z) = 0.117$, and added in quadrature to the previous PDF uncertainty.

As Z + jets is not normalised to data in a dedicated CR but to its nominal SM cross section, an additional normalisation uncertainty corresponding to the uncertainty on the cross section is thus considered.

Other backgrounds

For diboson, multiboson and $t\bar{t} + V$ processes, uncertainties arising from the unphysical scales μ_F, μ_R as well as μ_{QSF} and the CKKW ME+PS matching scale are considered using the same prescription described above for W/Z + jets. For these three processes as well as for the other minor backgrounds $V + h$ and $t\bar{t} + h$, an additional uncertainty on the SM cross section used for normalisation is considered.

7.2.2 Signal

Theoretical uncertainties on the SUSY signal processes arise from the unphysical factorisation, renormalisation and CKKW-L ME+PS merging scales. These are evaluated using a similar procedure as for background processes, varying the different scales up and down by a factor of two and comparing the expected signal rates. An additional uncertainty on PS originating from the chosen Pythia8 tune is estimated by varying up and down the chosen value for α_s^{ISR}.

As detailed in section 4.3.1, the cross section of electroweakino pair production is calculated using Resummino. A theoretical uncertainty on the cross section is considered in the following, but does not enter the statistical fit procedure as nuisance parameter. Instead, in addition to the set of observed CL_s values using the nominal cross section, two additional *variational* sets are derived using signal cross sections fixed at their $\pm 1\sigma$ variations. This allows to draw a cross section uncertainty band on the observed exclusion contour.

Due to the large number of MC samples, all theory uncertainties on SUSY signal processes are evaluated at truth-level only. As the VRs typically have relatively low signal contamination and thus low signal MC statistics available for evaluating theory uncertainties, requirements on observables with negligible impact on the shapes of the theoretical uncertainties are loosened. In the on-peak VRs, the requirements loosened are $m_{\mathrm{T}} > 60\,\mathrm{GeV}$ and $E_{\mathrm{T}}^{\mathrm{miss}}140\,\mathrm{GeV}$. The same loosened selection is applied in SRs in cases where MC statistical uncertainty is too high for a reliable estimation of the theoretical uncertainties. In the off-peak VRs, the requirements loosened are $m_{\mathrm{T}} > 60\,\mathrm{GeV}$ and $E_{\mathrm{T}}^{\mathrm{miss}} > 60\,\mathrm{GeV}$ and $m_{\mathrm{CT}} > 60\,\mathrm{GeV}$. Overall, the theoretical uncertainties on the expected signal rate range from about 10% in phase space regions with large mass splitting between $\tilde{\chi}_1^{\pm}/\tilde{\chi}_2^0$ and $\tilde{\chi}_1^0$ to about 25% in regions with small mass splittings.

7.3 Impact on signal regions

Table 7.1 shows a breakdown of the dominant systematic uncertainties on the background prediction in the SRs, obtained after a background-only fit in the CRs with subsequent extrapolation to the SRs. The total uncertainty in the SRs amounts to 15% in SRLM and increases to 25% in SRMM and 34% in SRHM. Theoretical uncertainties have the largest contribution to the total uncertainty. For SRLM, the largest uncertainty originates from the $t\bar{t}$ parton shower uncertainty (10%), while for SRMM (SRHM) the single top generator uncertainties are the largest ones with 10% (21%). Theoretical uncertainties on W + jets and other minor backgrounds have only small to negligible effects. The experimental uncertainties in general have less impact on the total uncertainty than the theoretical ones, with the largest experimental uncertainties contributing only 5–10% depending on the SR. The dominant experimental uncertainties arise from the JES and JER as well as $E_{\mathrm{T}}^{\mathrm{miss}}$ modelling and pile-up. The MS statistical uncertainties contribute 5–18% depending on the SR.

Table 7.1: Breakdown of the dominant systematic uncertainties in background estimates in the various exclusion signal regions (m_{CT} bins summed up). As the individual uncertainties can be correlated, they do not necessarily add up in quadrature to the total background uncertainty. The percentages show the size of the uncertainty relative to the total expected background. Table adapted from Ref. [170].

Signal Region	SRLM	SRMM	SRHM
Total background expectation	27	8.6	8.1
Total uncertainty	±4 [15%]	±2.2 [25%]	±2.7 [34%]
Theoretical systematic uncertainties			
$t\bar{t}$	±2.6 [10%]	±0.6 [7%]	±0.33 [4%]
Single top	±0.8 [2.7%]	±1.1 [12%]	±1.9 [23%]
W+jets	±0.23 [0.9%]	±0.07 [0.8%]	±0.19 [2.3%]
Other backgrounds	±0.13 [0.5%]	±0.15 [1.7%]	±0.08 [1.0%]
MC statistical uncertainties			
MC statistics	±1.7 [6%]	±1.1 [13%]	±1.2 [14%]
Uncertainties in the background normalisation			
Normalisation of dominant backgrounds	±1.3 [5%]	±1.6 [18%]	±1.3 [16%]
Experimental systematic uncertainties			
$E_{\mathrm{T}}^{\mathrm{miss}}$/JVT/pile-up/trigger	±1.8 [7%]	±0.4 [4%]	±0.4 [5%]
Jet energy resolution	±1.6 [6%]	±0.5 [6%]	±0.4 [5%]
b-tagging	±1.1 [4%]	±0.29 [3.4%]	±0.13 [1.5%]
Jet energy scale	±0.9 [3.2%]	±0.9 [10%]	±0.29 [4%]
Lepton uncertainties	±0.32 [1.2%]	±0.09 [1.0%]	±0.19 [2.3%]